Mon. Not. R. Astron. Soc. **000**, 1–6 (2010) Printed 24 February 2024 (MN LATEX style file v2.2)

A proper motion study of the globular cluster M55

K. Zloczewski[1⋆], J. Kaluzny[1] and I. B. Thompson[2]
[1] *Nicolaus Copernicus Astronomical Center, ul. Bartycka 18, 00-716 Warsaw, Poland*
[2] *The Observatories of the Carnegie Institution of Washington, 813 Santa Barbara St., Pasadena, CA 91101*

arXiv:1103.1733v1 [astro-ph.GA] 9 Mar 2011

Accepted 2010 – –. Received 2010 – –; in original form 2010 – –

ABSTRACT
We have derived the absolute proper motion (PM) of the globular cluster M55 using a large set of CCD images collected with the du Pont telescope between 1997 and 2008. We find ($\mu_\alpha cos\delta$, μ_δ) = (-3.31 ± 0.10, -9.14 ± 0.15) mas/yr relative to background galaxies. Membership status was determined for 16945 stars with $14 < V < 21$ from the central part of the cluster. The PM catalogue includes 52 variables of which 43 are probable members of M55. This sample is dominated by pulsating blue straggler stars but also includes 5 eclipsing binaries, three of which are main sequence objects. The survey also identified several candidate blue, yellow and red straggler stars belonging to the cluster. We detected 15 likely members of the Sgr dSph galaxy located behind M55. The average PM for these stars was measured to be ($\mu_\alpha cos\delta$, μ_δ)=(-2.23 ± 0.14, -1.83 ± 0.24) mas/yr.

Key words: astrometry – globular clusters: individual: NGC 6809 (M55) – binaries: eclipsing – blue stragglers – galaxies: individual: Sagitarrius dSph

1 INTRODUCTION

M55 (NGC 6809) is a metal-poor globular cluster (GC) in the Galactic halo (l = 9°, b = −23°), discovered by Nicholas Louis de Lacaille in 1752. Over 70 variable stars are known in the field of the cluster (Clement et al. 1999; Olech et al. 1999; Pych et al. 2001; Kaluzny et al. 2010, hereafter JK10). About half of these are located in the blue straggler region of the color-magnitude diagram (CMD) and 13 are RR Lyr type pulsators. The cluster is close to us ($(m-M)_V = 13.87$; Harris 1996) and is relatively sparse. This makes it an ideal target for a measurement of the cluster proper motion (PM). Several authors have shown that for nearby GCs ground based CCD observations with temporal baselines of 3-5 years are sufficient to efficiently separate member stars from field interlopers (Anderson et al. 2006; Yadav 2008; Bellini et al. 2009; Montalto et al. 2009).

In Sec. 2 we describe the observational data and methods used to prepare CCD images for the analysis. The procedures employed for the determination of relative PMs of individual stars and for the determination of the absolute PM of the cluster are presented in Sec.3. A discussion of our results is given in Sec. 4 and this is followed by a Summary.

2 DATA SELECTION AND PREPARATION

The images of M55 analyzed in this paper were selected from the data collected by the Cluster AgeS Experiment (CASE; Kaluzny et al. 2005) project during the period 1997–2008. Observations were made with the 2.5-m du Pont telescope at Las Campanas Observatory. All images were obtained with the same detector and the same set of filters. We used the $2K^2$ Tek#5 CCD camera with a scale of 0.259″/pixel and a field of view of 530″×530″. CASE observed M55 as part of a program to obtain follow-up photometric observations of specific variables and to survey the central part of the cluster for detached eclipsing binaries. For the present analysis we selected four pointings, named F1-F4. The locations of these fields are shown in Fig. 1. The field centers are at the following (RA, Dec) coordinates for Epoch 2000: F1 (294.9975°, −30.9621°), F2 (294.9788°, −30.9316°), F3 (294.9668°, −30.9499°) and F4 (295.0200°, −30.9707°). The set of frames selected for a given observing run and for a given pointing is called a 'data-set'. Each data-set includes the V frames with the best seeing obtained for a given observing run. We considered only frames with seeing better than 1.1″and obtained at an air-mass less than 1.1, avoiding observation obtained through clouds or with a bright sky. A summary of the final data-sets is given in Table 1.

For each data set we constructed an averaged, high signal-to-noise ratio frame using the DIAPL[1] package. In

⋆ E-mail: kzlocz@camk.edu.pl (KZ); jka@camk.edu.pl (JK); ian@obs.carnegiescience.edu (IBT);

[1] DIAPL – Difference Image Analysis PL

brief, individual frames were transformed to the coordinates of a chosen reference image. The point spread function (PSF) of each frame was also transformed to match the PSF of the reference image (i.e.the transformation kernel between a given frame and the reference image was derived). The best seeing frame from a given data-set served as the reference image. The transformed frames were subsequently stacked by averaging to form what we later call an 'average frame'. During this procedure the reference as well as the individual frames were divided into 16 overlapping sub-frames to reduce effects of PSF variability.

We decided to obtain PMs for stars detected on the averaged frames of fields F1 and F2 for seasons 1997 and 1999, respectively. These frames are characterized by particularly good seeing and high S/N. We label these the 'master' frames. The observations of fields F1 and F2 span 9 and 11 years, respectively. Fields F1 and F2 show significant overlap with fields F3 and F4. Therefore, most of stars detected on F1-1997 and F2-1999 images are present on the remaining averaged frames. A master list of stars was extracted from frames F1-1997 and F2-1999 using the DAOPHOT/ALLSTAR package (Stetson 1987). The reductions were made on 16 overlapping sub-frames resulting from a 4x4 division of the respective averaged frames. A Moffat function with linear spatial variability was used to characterize the PSF. Due to crowding the photometry was extracted in an iterative way, gradually decreasing the detection threshold. An effort was made to avoid artificial splitting of bright stars which can happen when one uses an automatic procedure to detect missed objects in star subtracted images. During the last iteration the residual images were inspected by eye to find previously undetected stars. The master lists contained 47333 and 42725 objects for fields F1 and F2, respectively. In the next step these lists were transformed to the coordinates of the *averaged frames* for different epochs. Profile photometry (as well as PSF modeling) was measured for these frames with ALLSTAR parameter set to $re = 1$. In this way the positions of objects from the master lists have been re-determined for a given averaged frame. As before, we used a 4×4 mosaic of sub-frames for actual reductions.

3 PROPER MOTIONS

3.1 Proper motion measurements

Relative PMs of individual stars were derived from their positions measured at different epochs with respect to nearby cluster stars. This was done using a procedure resembling that described by Anderson et al. (2006). As a first guess we selected as cluster stars objects located along the main sequence and red giant and horizontal branches on the CMD. For this purpose we constructed deep $V/(V-I)$ CMD's for both analyzed fields, including only stars with high quality photometry. The photometric quality was judged based on CHI and SHARP fit parameters returned by ALLSTAR. PM measurements were only made for stars with $V < 21.0$.

For any given star we selected a set of 'grid stars' located inside an $\sim 80'' \times 80''$ square, centered on the star to be measured. Only likely cluster members were considered at this step. The median number of grid stars was equal to 203 for F1 and 202 for F2. The grid stars were used to calculate the local geometrical transformation between the appropriate master frame and a given average frame. This transformation was calculated using the IRAF[2] *immatch.geomap* and *immatch.geoxytran* tasks. We used a two-dimensional 3rd order Chebyshev polynomial as the transformation function. Subsequently, we calculated the expected coordinates (X_C, Y_C) of the star on the average frame based on its (X_0, Y_0) coordinates on the master frame. The relative motion was derived as the difference between the calculated and observed coordinates: $dX = X_C - X_0$ and $dY = Y_C - Y_0$. The shifts dX and dY were measured for all suitable average frames. Finally, the PM of a given star was calculated by a linear fit to dX and dY as a function of time. Figure 2. shows as an example the PM measurement for star #13300383.

Individual points were weighted by the amount of flux corresponding to a given 'average frame'. In practice this was done by summing fluxes measured for several bright isolated stars on individual frames before averaging. We then took the inverse value of the summed flux to compute the relative weight for each 'average frame'. PM measurements were only attempted for objects with positions determined on at least four epochs spanning at least 4 years. We retained only those objects for which the significance of a linear fit to the PM exceeded 99% (i.e. a χ^2 test was performed with a false detection rate of $\alpha = 1.0$ %).

PM measurements were performed in two steps. In the first step we made preliminary PM estimates. In the second step we used only reference stars for which reliable PMs were obtained in step one. Additionally, positions of reference stars were shifted back to the reference epoch (F1-1997 or F2-1999) to minimize errors due to the movement of 'grid stars'. These new positions were used to calculate geometrical transformations in the second iteration. Figure 3 shows that the total RMS of the geometrical transformation does not change significantly with time and is weakly seeing-dependent.

Equatorial coordinates for the measured stars were obtained using frame astrometric solutions based on a set of stars selected from the UCAC3 catalogue (Zacharias et al. 2010). We considered only stars with $V < 17$ which resulted in 671 and 636 stars for fields F1 and F2, respectively. The average residual of the adopted solutions is 0.15 arcsec. Our catalog of M55 stars includes a total of 16954 stars with a measured relative PM. Table 3 presents the first few lines of the complete catalogue which is available in electronic form at `html://case.camk.edu.pl`.

3.2 Error estimates

Figure 4 shows the difference in measured PMs for 11398 stars measured on both fields F1 and F2. For 66% of these

`http://users.camk.edu.pl/pych/DIAPL` developed by W. Pych)

[2] IRAF is distributed by the National Optical Astronomy Observatory, which is operated by the Association of Universities for Research in Astronomy, Inc., under a cooperative agreement with the National Science Foundation.

stars the difference is smaller than $\Delta\mu = 0.34$ mas/yr. This can be adopted as a robust estimate of the average error of a PM determination for the whole sample. For 95% of the stars the difference is smaller than $\Delta\mu = 0.94$ mas/yr.

Figure 5 shows the dependence of $\log_{10}\sigma_\mu$ on V magnitude. For stars with $V \approx 19.0$ the median value of σ_μ is equal to 0.47 mas/yr. At $V = 20$ the median value of σ_μ reaches 0.65 mas/yr. An increased scatter in σ_μ can be noted for $V < 14.5$. This arises from the saturation of bright stars on some frames resulting in fewer available epochs for the PM measurement. Note that the σ_μ values below $V \approx 17.5$ arise due to systematic effects and for fainter magnitudes are related to photon noise statistics. The spread of the σ_μ values may be due to the methodology of the reductions (fitting and coordinate transformations) and to the number of points used in the astrometric solutions.

3.3 Completeness

We assessed the completeness of our PM survey as a function of V magnitude and radial distance from the cluster center. Completeness was defined as the ratio of the number of stars with final PM measurements to the number of stars for which we attempted to make a PM measurement. The results are shown in graphical form in Figs. 6 and 7. Only points with relative uncertainty smaller than 20% were plotted. The completeness exceeds 70% for $13 < V < 17$ and drops to 25% at $V = 20.0$. As expected, the completeness increases with distance from the cluster center, flattening at a distance of about 4 arcmin. The larger incompleteness observed at the cluster center is due to effects associated with crowding. The apparent peak at $d = 4$ arcmin, evident for all magnitude ranges, results from the fact that for more distant stars often only a few epochs were available. No attempt was made to estimate the completeness of the initial master list of stars detected in the studied field.

3.4 Cluster membership probabilities

A vector point diagram (VPD) including 16945 stars with reliably derived relative PMs is presented in Fig. 8. Only 2.3% (394 objects) of the measured objects have $\mu > 3.0$ mas/yr and these are likely field stars. To estimate the probability that a star is a cluster member we use the 'local-sample method' described in Platais (1984) with further improvements proposed by Platais et al. (2003). In our case, however, field stars comprise only a very small fraction of the total sample.

We therefore decided to assign stars to one of three groups based on location in the VPD diagram and on the error of the measured PM. All objects with a measured PM were divided into five sub-samples in magnitude: $13 < V < 17$ (N = 1048), $17 < V < 18$ (N = 2511), $18 < V < 19$ (N = 5140), $19 < V < 20$ (N = 5715) and $20 < V < 21$ (N = 2531). For each bin we selected stars with $\mu < 1.8$ mas/yr and calculated for these average values and standard deviations of $\mu_\alpha cos\delta$ and μ_δ (M_α, M_δ, S_α, S_δ). The total value of the standard deviation of the PM was then calculated as $S = (S_\alpha^2 + S_\delta^2)^{1/2}$. Average values and standard deviations of th eindividual errors of $\mu_\alpha cos\delta$ and μ_δ were also calculated ($ME_{\alpha,\delta}$, $SE_{\alpha,\delta}$). Subsequently, the total values $ME = (ME_\alpha^2 + ME_\delta^2)^{1/2}$ and $SE = (SE_\alpha^2 + SE_\delta^2)^{1/2}$ were calculated. The results are listed in Table 2. The histograms showing the distribution of both components of PM for the brightest and for the faintest bin in V are shown in Fig. 9. Stars were assigned to three classes of membership. Those with $M > 3.0 \times S$ are considered non-members (mem=0; N = 379). Possible members (mem=1; N = 187) are stars which $M \leqslant 3 \times S$ but with $\sigma_\mu > ME + 3.0 \times SE$). Objects with $M \leqslant 3 \times S$ and $\sigma_\mu \leqslant ME + 3.0 \times SE$ are considered PM members of the cluster (mem=2; N = 16379). The membership class defined as above is listed in 12-th column of Table 3.

3.5 Absolute proper motions

Among the objects remaining on the star-subtracted averaged frames there are a number of relatively faint, unresolved galaxies. These were selected by visual inspection of both the *averaged frames* and *averaged frames* with stars subtracted. The sample includes a total of 70 galaxies from fields F1 and F2. Eleven of these are undoubtedly relatively bright compact galaxies. Due to crowding of the stellar field we decided to extract photometry of the galaxies simultaneously with photometry of the nearby stars using the GALFIT 3.0 code (Peng et al. 2010). This was done on (30×30 or 60×60 pixel^2) sub-frames centered on a given galaxy and extracted from the relevant averaged frame.

For every sub-image a PSF model was constructed using a few bright stars and IRAF's daophot routines. All but two of the galaxies were modeled with a 2-D Sersic function. The fit included the closest stars, some of which were present in galaxy foreground. The sky background was also fitted. The coordinates of the galaxies derived this way were used to calculate their PMs relative to the cluster. This was done using the same procedure we applied earlier to stars. We excluded two galaxies from the sample since their dX and dY shifts showed non-linear dependence on time. We interpret this as due to problems with the proper determination of their coordinates. The weighted average of the relative PM based on the remaining 9 galaxies is ($\mu_\alpha cos\delta$, μ_δ) = (-3.19 ± 0.37, -9.27 ± 0.80) mas/yr. Kaluzny et al. (2005) in their search for cataclysmic variables in M55 identified 7 blue stellar-like objects. One of those, M55-B1, was classified as QSO based on its light curve. The object is present in our catalogue as #23100322 with a PM value similar to the average PM of our sample of 9 galaxies. Another blue object, #22401066 (#17550 in the Kaluzny et al. 2005 numbering of their reference frame), has a PM indicating that it is a cluster member. We failed to obtain PMs for the remaining 5 blue stellar-like objects from Kaluzny et al. (2005) because they are too faint. The weighted average PM based on 9 galaxies and M55-B1 is ($\mu_\alpha cos\delta$, μ_δ) = (-3.30 ± 0.20, -9.14 ± 0.17) mas/yr. A VPD for these 10 objects is shown in Fig. 10. The point with the largest uncertainty corresponds to an edge-on galaxy. After dropping this object we obtained ($\mu_\alpha cos\delta$, μ_δ) = (-3.31 ± 0.10, -9.14 ± 0.15) mas/yr. This value was obtained assuming ($\mu_\alpha^c cos\delta$, μ_δ^c) = (0.0,0.0) mas/yr. Our value can be compared with result of Dinescu et al. (1999) who obtained a PM for M55 of (-1.57 ± 0.62, -10.14 ± 0.64) mas/yr. Their measurement was obtained using wide-field photographic plates with a base-line of 25 years.

4 DISCUSSION

4.1 Color-magnitude diagram

Figure 11 shows a $V/(B-V)$ CMD of M55 based on photometry from JK10. The left panel includes about 10 thousands stars with good quality photometry. By selecting stars classified as certain PM members (mem=2 in Table 3) we obtained the CMD shown in the right panel of Fig. 11.

4.2 Binary stars

A clear sequence running parallel to the main-sequence can be seen in the cleaned CMD. We interpret these objects to be binary stars in M55. The binary content of M55 was discussed at length by Sollima et al. (2007). These authors used HST/ACS images centered on the cluster core. Our data show that a population of binaries with $q \approx 1$ is also present in the more external parts of M55. The binary sequence crosses the cluster turn-off and then extends to the blue including several candidate blue straggler (BS) stars. In addition to the BSs we note the presence of candidate yellow and red straggler stars. These objects are located above the main-sequence turnoff on both sides of the lower part of the subgiant branch. A definitive determination of the membership status of these red/yellow/blue stragglers can be made based on measurements of their radial velocities. M55 has a large radial velocity, $V_{rad} = 174.8$ km/s (Harris 1996), and it should be easy to separate field stars from cluster members with high confidence.

4.3 Variable stars and blue stragglers

Our PM survey can be used to assign tentative membership for variables and for other interesting objects from the cluster field. We compiled a list of variables and candidate blue stragglers from Olech et al. (1999), Pych et al. (2001), Lanzoni et al. (2007) & JK10. Our PM catalog includes 52 out of 71 known variables and 46 out of 65 candidate BSs. These stars are listed in Table 4. In Fig. 12 we present a CMD of M55 showing the upper main-sequence and BS regions. All variable BSs with available PMs turned out to be probable members of the cluster. The BS region contains some PM members of M55 not known to be variables. The light curves of these stars obtained by JK10 were re-examined in detail but none of them showed any evidence for variability. Two of the variable BSs are eclipsing binaries. Variables which with high confidence do not belong to the cluster are: V15, V49, V50 and V51. In addition the BSs BSS-7, BSS-27, BSS-31 & BSS-39 from Lanzoni et al. (2007) are probable field stars. Individual cases should be checked taking into account individual PM errors. Further radial velocity studies of all variable stars are needed to reliably establish their membership and evolutionary status.

4.4 Sagittarius dSph

The variable V15 has been found by Olech et al. (1999) to be an RR Lyr star belonging to the Sagittarius dSph galaxy. Part of this extended galaxy is present in the background of M55 (Ibata, Gilmore, & Irwin 1994; Mateo et al. 1996). We measured the PM of V15 to be ($\mu_\alpha cos\delta$, μ_δ)=(1.14 $\pm$ 0.31, 7.81 $\pm$ 0.36) mas/yr. The variable is located on the VPD inside an apparent clump formed by a few dozen stars. We identify this group of stars as likely members of the Sagittarius dwarf. For 29 stars surrounding V15 on the VPD we obtained a weighted mean absolute PM of ($\mu_\alpha cos\delta$, μ_δ)=(-2.23 ± 0.14, -1.83 ± 0.24) mas/yr. This position in the VPD was calculated iteratively with the PM of V15 as a starting point and using stars within a circle of radius of $r = 1$ mas/yr. The measured value of the average PM does not change beyond the quoted errors if this procedure is repeated for radii of 0.75 and 1.25 mas/yr. The positions of these stars on the cluster CMD are shown in Fig. 11. We conclude that this subsample is composed of upper main-sequence and subgiant stars from the Sagittarius dwarf galaxy. For a comparison, Pryor et al. (2010) determined the absolute PM of the Sagittarius dwarf to be $(\mu_\alpha cos\delta, \mu_\delta) = (-2.75 \pm 0.20, -1.65 \pm 0.22)$ mas/yr based on archival HST images. Their measurement was made at positions located 7.3 & 9.7 deg NW from the center of M55. Earlier determinations of the PM for the galaxy were reported by Dinescu et al. (2005) and by Ibata et al. (1997).

5 SUMMARY

We have performed the first proper motion study of the globular cluster M55 based on ground-based CCD images. Relative PMs were derived for 16945 stars to $V < 21.0$ over a temporal baseline of up to 11 years. We assigned a cluster memberships status for all stars with available PM measurements. The absolute PM of M55 was measured to be ($\mu_\alpha cos\delta$, μ_δ) = (-3.31 ± 0.10, -9.14 ± 0.15) mas/yr. The absolute PM was derived for a portion of the Sagittarius dSph galaxy located in the background of the cluster. The results of our survey allow a selection of cluster variables, as well as cluster blue/yellow/red stragglers, with high certainty.

ACKNOWLEDGMENTS

KZ & JK were supported by the Foundation for Polish Science through grant MISTRZ, by the grant N N203 379936 and N N203 406139 from the Ministry of Science and Higher Education. I.B.T acknowledges the support of NSF grant AST-0507325. We thank Dr. F. van Leeuwen for detailed and helpful comments on an earlier version of this paper. We thank M. Rozyczka for a careful reading of the manuscript.

REFERENCES

Anderson, J., Bedin, L. R., Piotto, G., Yadav, R. S., Bellini, A., 2006, A&A, 454, 1029

Bellini, A., Piotto, G., Bedin, L. R., Anderson, J., Platais, I., Momany, Y., Moretti, A., Milone, A. P., Ortolani, S., 2009, A&A, 493, 959

Clement, Ch.M., Muzzin, A., Dufton, Q., Ponnampalam, T., Wang, J., Burford, J., Richardson, A., Rosebery, T., Rowe, J., Hogg, H.S., 2001, AJ, 122, 2587

Dinescu, D.I., van Altena, W.F., Girard, T.M., Lopez, C.E., 1999, AJ, 117, 277

Dinescu, D.I., Girard, T.M., van Altena, W.F., Lopez, C.E., 2005, ApJ, 618L, 25

Harris, W.E., 1996, AJ, 112, 1487

Girard, T.M., Grundy, W.M., Lopez, C.E., van Altena, W.F., 1989, AJ, 98, 227

Ibata R.A., Gilmore G.F., & Irwin M.J. 1994, Nature 370, 194

Ibata R.A., Wyse R.F.G., Gilmore G.F., Irwin M.J., Suntzeff, N.B. 1997, AJ 113, 634

Kaluzny, J., Thompson, I.B., Krzeminski, W., Preston, G.W., Pych, W., Rucinski, S.M., Schwarzenberg-Czerny, A., Shectman, S.A., Stachowski, G., 2005, AIPC (eds. J.Mikolajewska, A.Olech), 752, 70

Kaluzny, J., Pietrukowicz, P., Thompson, I.B., Krzeminski, W., Schwarzenberg-Czerny, A., Pych, W., Stachowski, G., 2005, MNRAS, 359, 677

Kaluzny, J., Thompson, I.B., Krzeminski, W., Zloczewski, K., 2010, Acta Astronomica, 60, 245

Lanzoni, B., Dalessandro, E., Perina, S., Ferraro, F.R., Rood, R.T., Sollima, A., 2007, ApJ, 670, 1065

Mateo, M., Mirabal, N., Udalski, A., Szymański, M., Kaluzny, J., Kubiak, M., Krzemiński, W., & Stanek, k. z., 1996, ApJ, 458, L13

Montalto, M., Piotto, G., Desidera, S., Platais, I. Carraro, G., Momany, Y., de Marchi, F., Recio-Blanco, A., 2009, A&A, 505, 1129

Olech, A., Kaluzny, J., Thompson, I. B., Pych, W., Krzeminski, W., Shwarzenberg-Czerny, A., 1999, AJ, 118, 442O

Peng, C.Y., Ho, L.C.; Impey, C.D.; Rix, H-W, 2010, AJ, 139, 2097

Platais, I. K., 1984, Soviet Astronomy Letters, 10, 203

Platais, I., Kozhurina-Platais, V., Mathieu, R.D., Girard, T.M., van Altena, W.F., 2003, AJ, 126, 2922

Pryor, C., Piatek, S., Olszewski, E.W., 2010, AJ, 139, 839

Pych, W., Kaluzny, J., Krzeminski, W., Schwarzenberg-Czerny, A., Thompson, I.B., 2001, A&A, 367, 148

Sollima, A., Beccari, G., Ferraro, F.R., Fusi Pecci, F., Sarajedini, A., 2007, MNRAS, 380, 781

Stetson, P.B., 1987, PASP, 99, 191

Yadav, R.K.S., Bedin, L.R., Piotto, G., Anderson, J., Cassisi, S., Villanova, S., Platais, I., Pasquini, L., Momany, Y., Sagar, R., 2008, A&A, 484, 609

Zacharias, N., Finch, C., Girard, T., Hambly, N., Wycoff, G., Zacharias, M.I., Castillo, D., Corbin, T., DiVittorio, M., Dutta, S., and 20 coauthors, 2010, AJ, 139, 2184

Table 1. Summary of M55 observations used in this study.

dataset	<HJD-2450000.0> [yr]	N	<exptime> [s]	<seeing> [″]
F1-1997	1.65	12	60	0.80
F1-2006	10.70	6	75	1.06
F1-2007	11.86	8	40	1.08
F1-2008	12.66	21	35	0.90
F2-1999	3.68	23	120	0.83
F2-2001	5.65	8	100	0.93
F2-2003	7.58	18	85	0.86
F2-2004A	8.63	3	80	1.05
F2-2004B	8.78	17	50	0.89
F2-2006A	10.57	19	40	0.70
F2-2006B	10.64	15	60	0.87
F2-2008	12.68	14	50	0.67
F3-2006A	10.71	8	65	0.82
F3-2006B	10.72	7	50	0.83
F3-2007A	11.70	4	60	0.95
F3-2007B	11.77	13	60	0.78
F3-2008	12.73	14	85	0.89
F4-2007	11.75	18	60	0.82

Table 2. PM statistics for magnitude bins. Only stars with $\mu <$ 1.8 were used. See text for details.

V	M_α	M_δ	S_α	S_δ	ME	SE
13–17	0.038	-0.010	0.308	0.324	0.268	0.152
17–18	0.022	-0.010	0.346	0.362	0.294	0.185
18–19	-0.000	-0.019	0.408	0.414	0.396	0.195
19–20	-0.002	-0.010	0.512	0.514	0.555	0.175
20–21	0.023	-0.024	0.644	0.658	0.710	0.162

This paper has been typeset from a TEX/ LATEX file prepared by the author.

Table 3. First lines of the electronically available PM catalogue. Columns: (1) star ID (starting with 1 and 2 for fields F1 and F2, respectively); (2) & (3) equatorial coordinates $(\alpha, \delta)_{2000.0}$ for epochs 1997.41 and 1999.46 for F1 and F2, respectively; (4) & (5) XY pixel coordinates on reference frames; (6)–(9) PMs and their errors; (10) number of epochs used; (11) temporal baseline; (12) cluster membership (for explanation see Sec. 3.4); (13) V magnitude.

ID	α	δ	X	Y	$\mu_\alpha cos\delta$	$\sigma_{\mu_\alpha cos\delta}$	μ_δ	σ_{μ_δ}	N	dT	mem	V
(1) [#]	(2) [°]	(3) [°]	(4) [pixel]	(5) [pixel]	(6) [mas/yr]	(7) [mas/yr]	(8) [mas/yr]	(9) [mas/yr]	(10) [#]	(11) [yr]	(12) [-]	(13) [mag]
11100007	295.053729	-30.902151	449.000	149.951	0.25	0.22	-0.51	0.29	8	10.217	2	14.586
11100009	295.058880	-30.928524	362.498	509.429	-0.66	0.22	11.84	0.19	9	11.033	0	14.810
11100020	295.066402	-30.924406	277.438	446.329	-0.05	0.17	0.65	0.21	5	11.017	2	16.792
11100021	295.060880	-30.928912	338.443	513.105	-0.36	0.32	1.24	0.16	9	11.025	2	16.796
11100023	295.046117	-30.915949	525.736	346.697	0.53	0.52	-0.31	0.79	13	10.217	1	16.980
11100026	295.071004	-30.916422	230.649	332.343	0.47	0.20	0.06	0.20	5	11.017	2	17.029
11100032	295.066432	-30.905801	295.049	189.641	0.09	0.14	0.15	0.22	6	11.017	2	17.223
11100039	295.056244	-30.921224	400.756	410.949	-0.10	0.11	-0.20	0.11	9	11.025	2	17.359
11100045	295.047850	-30.924146	497.279	458.297	-0.01	0.06	-0.22	0.14	11	11.033	2	17.441
11100046	295.070611	-30.926622	225.463	473.366	-0.61	0.15	0.88	0.07	5	11.017	2	17.455

Table 4. Tentative membership status (mem) for variables and for BSs from Lanzoni et al. (2007; ID_L).

ID	ID_L	ID_{PM}	mem	ID	ID_L	ID_{PM}	mem	ID	ID_L	ID_{PM}	mem
V02	—	24300001	2	V32	BSS-21	22400204	2	V62	—	23201072	2
V04	—	12200014	2	V33	BSS-51	13400039	2	V63	BSS-35	23300072	2
V05	—	22405193	2	V34	BSS-61	12400077	2	V64	—	23300099	2
V06	—	12200010	2	V35	BSS-52	23200027	2	V65	—	13300228	2
V07	—	12220322	2	V36	BSS-53	23300087	2	V67	—	14400131	2
V08	—	22400024	2	V37	BSS-55	13300163	2	V69	BSS-45	13400057	2
V10	—	12100004	2	V38	BSS-20	13300141	2	—	BSS-01	22300208	2
V11	—	21300008	2	V40	BSS-60	12200189	2	—	BSS-02	13200131	2
V12	—	12300018	2	V41	BSS-10	22400135	2	—	BSS-07	22300198	0
V15	—	14400150	0	V42	BSS-25	13200170	2	—	BSS-08	12300182	2
V16	BSS-56	12200151	2	V44	—	21400232	2	—	BSS-14	23400059	2
V17	BSS-58	11300070	2	V45	BSS-32	12200109	2	—	BSS-15	22300189	2
V18	BSS-22	21300093	2	V47	BSS-06	22300183	2	—	BSS-16	23300108	2
V19	BSS-12	22300308	2	V48	BSS-03	12200099	2	—	BSS-19	22400262	2
V20	BSS-23	23400089	2	V49	—	11300622	0	—	BSS-27	13400030	0
V21	BSS-26	22400085	2	V50	—	21400104	0	—	BSS-31	21400069	0
V22	BSS-54	12400055	2	V51	—	21200261	0	—	BSS-34	22200033	2
V23	BSS-62	13200171	2	V53	BSS-37	12300123	2	—	BSS-36	11300049	2
V24	BSS-57	23300107	2	V54	—	24300158	2	—	BSS-39	23100015	1
V25	BSS-50	23300058	2	V55	BSS-46	21300126	2	—	BSS-41	22203014	2
V26	BSS-63	23300063	2	V57	BSS-04	22300166	2	—	BSS-49	22200293	2
V27	BSS-24	23400103	2	V60	—	22300197	2				
V31	BSS-11	12300229	2	V61	—	12300228	2				

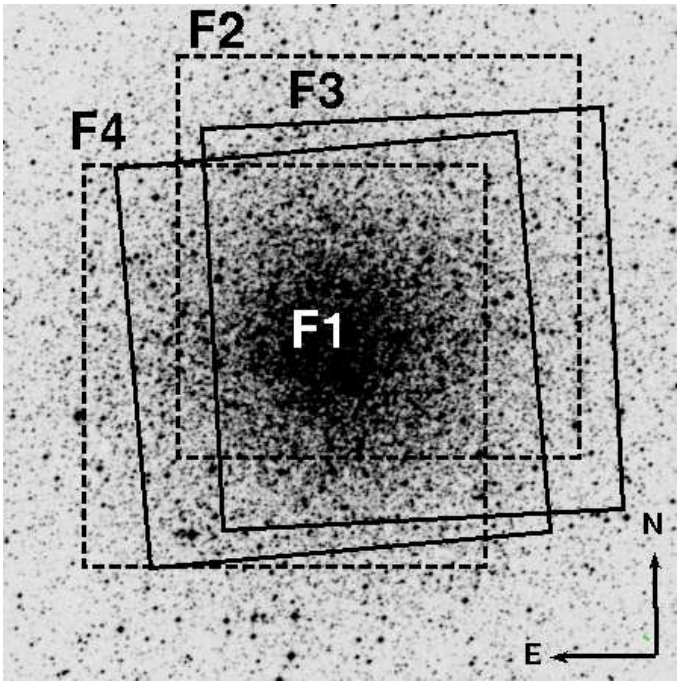


Figure 1. Positions of the F1, F2, F3, F4 fields overlaid on a DSS R-band image of M55. The field of view is $15' \times 15'$.

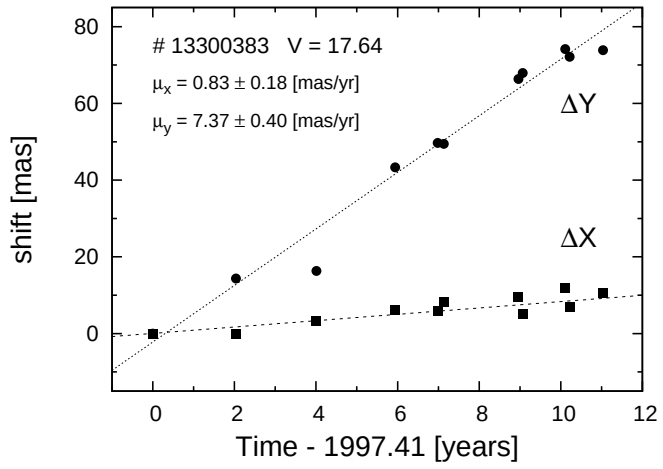


Figure 2. An example of PM determination for one of the fast moving stars.

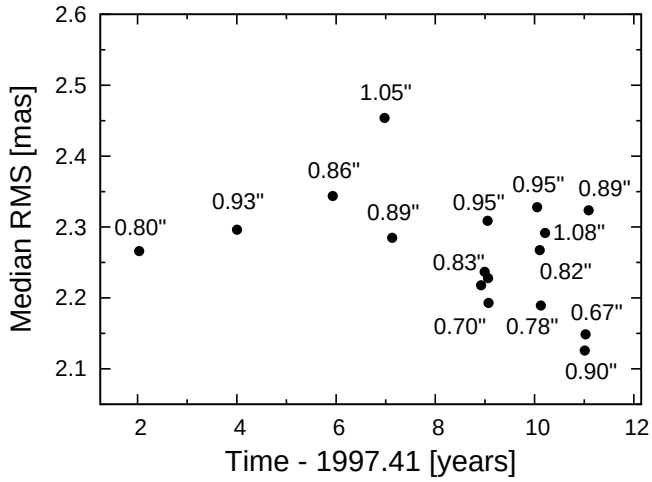


Figure 3. RMS of geometrical transformation versus time for field F1. Average seeing for a given frame is indicated.

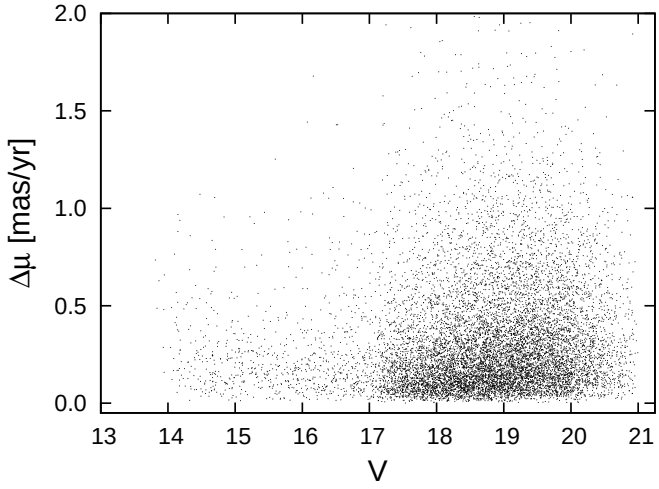


Figure 4. Differences of PMs measured for stars in common to fields F1 & F2 as a function of V magnitude.

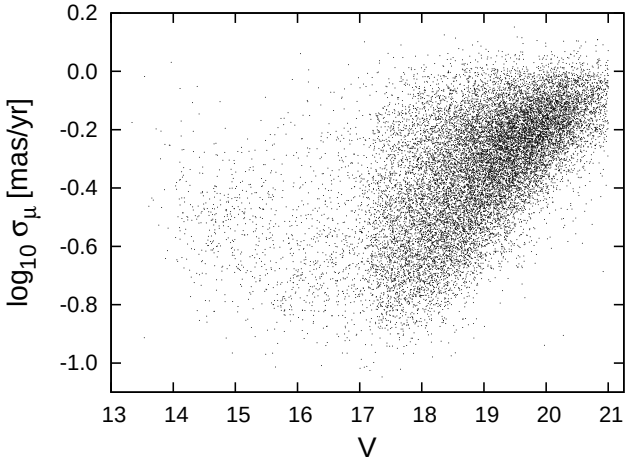


Figure 5. PM errors.

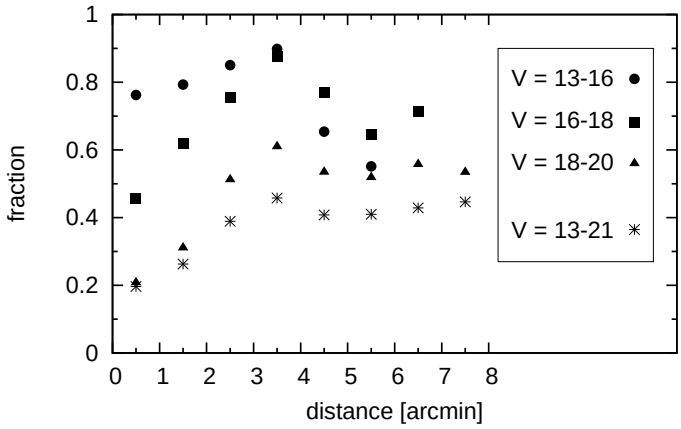


Figure 6. Completeness of the PM catalog as a function of projected distance from the cluster center.

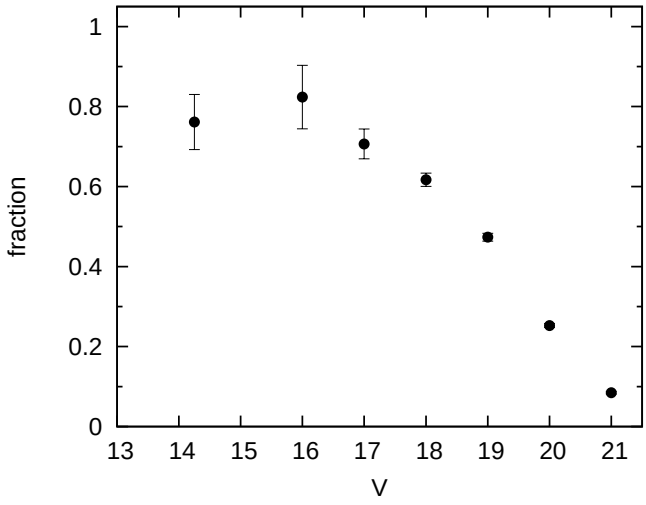


Figure 7. Completeness of the PM catalog as a function of V magnitude.

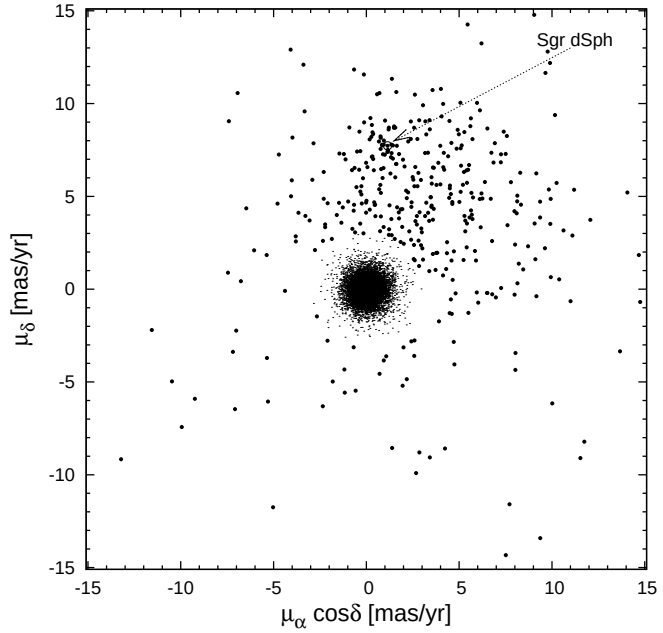


Figure 8. The proper motion Vector Point Diagram for 16945 stars from M55. The catalog includes 15 high velocity stars located outside of the plotted area. Stars with μ >3.0 are marked with large dots (394 objects). The arrow points to the clump of stars presumably associated with the Sgr dSph galaxy.

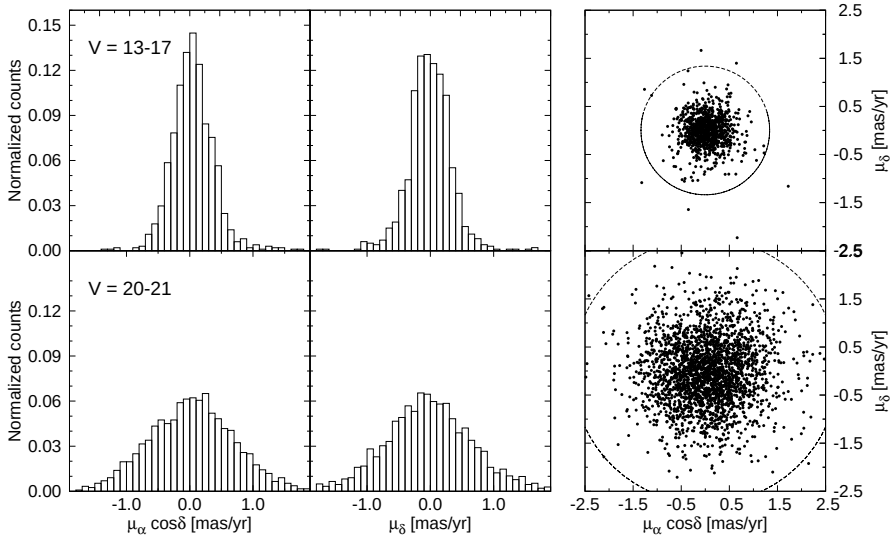


Figure 9. The distribution in $\mu_{cos\delta}$ and μ_δ for magnitude bins V = 13-17 and V = 20-21. The right panel shows a VPD for stars with PM < 1.8 mas/yr. Circles indicate 3×S which is defined in Sec. 3.4.

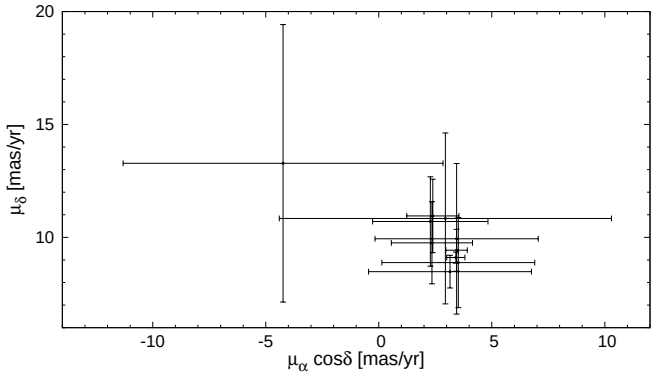


Figure 10. Relative PMs of 9 compact galaxies and the QSO M55-B1 measured with respect to M55 stars.

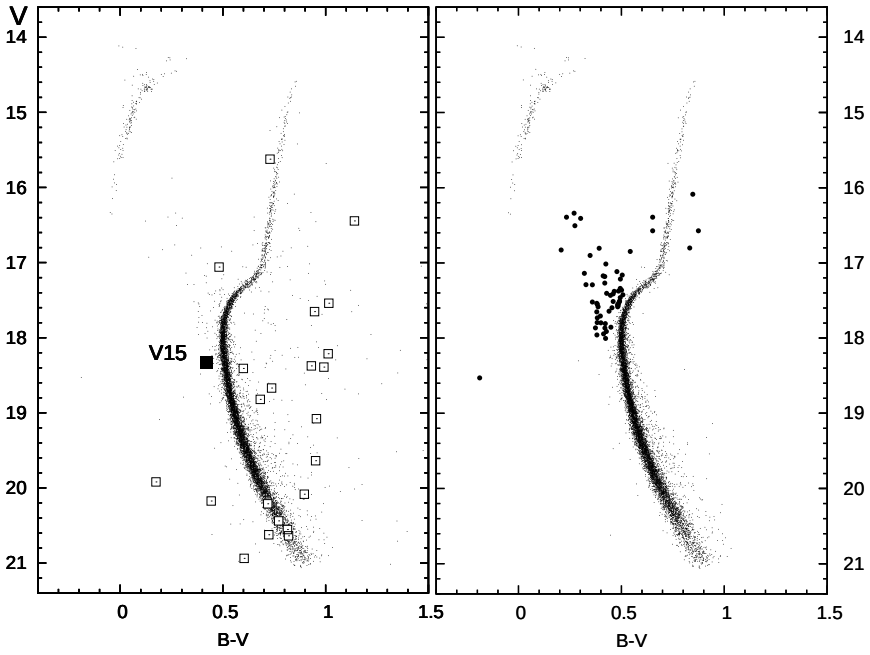


Figure 11. Left panel - $V/(B-V)$ CMD of M55 based on JK10 photometry. Stars selected as likely PM members of the Sgr dSph galaxy are marked with squares (see Sec. 4.3).; Right panel - the CMD including only probable cluster members. Candidate blue/yellow/red stragglers are marked with large dots.

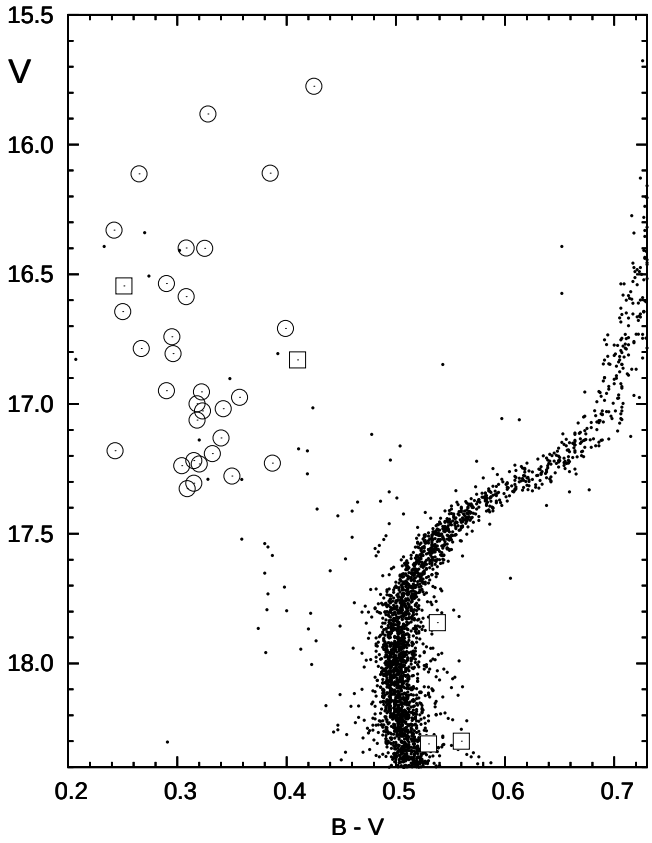


Figure 12. $V/(B-V)$ CMD showing the turnoff and BS regions of M55. Only likely cluster members are plotted. Circles - pulsating variables of SX Phe type; squares - eclipsing binaries.